Optimal streaks in the circular cylinder wake and suppression of the global instability

Gerardo del Guercio, Carlo Cossu, Grégory Pujals

▶ **To cite this version:**

Gerardo del Guercio, Carlo Cossu, Grégory Pujals. Optimal streaks in the circular cylinder wake and suppression of the global instability. Journal of Fluid Mechanics, 2014, 752, pp.572-588. 10.1017/jfm.2014.347 . hal-03520550

HAL Id: hal-03520550
https://hal.science/hal-03520550

Submitted on 11 Jan 2022

HAL is a multi-disciplinary open access archive for the deposit and dissemination of scientific research documents, whether they are published or not. The documents may come from teaching and research institutions in France or abroad, or from public or private research centers.

L'archive ouverte pluridisciplinaire **HAL**, est destinée au dépôt et à la diffusion de documents scientifiques de niveau recherche, publiés ou non, émanant des établissements d'enseignement et de recherche français ou étrangers, des laboratoires publics ou privés.

OATAO
Open Archive Toulouse Archive Ouverte

Open Archive TOULOUSE Archive Ouverte (OATAO)

OATAO is an open access repository that collects the work of Toulouse researchers and makes it freely available over the web where possible.

This is an author-deposited version published in : http://oatao.univ-toulouse.fr/
Eprints ID : 13921

To link to this article : DOI: 10.1017/jfm.2014.347
URL : http://dx.doi.org/10.1017/jfm.2014.347

To cite this version : Del Guercio, Gerardo and Cossu, Carlo and Pujals, Grégory *Optimal streaks in the circular cylinder wake and suppression of the global instability.* (2014) Journal of Fluid Mechanics, vol. 752. pp. 572-588. ISSN 0022-1120

Any correspondance concerning this service should be sent to the repository administrator: staff-oatao@listes-diff.inp-toulouse.fr

Optimal streaks in the circular cylinder wake and suppression of the global instability

Gerardo Del Guercio[1,2], Carlo Cossu[1,†] and Gregory Pujals[2]

[1]CNRS – Institut de Mécanique des Fluides de Toulouse (IMFT), Allée du Pr. Camille Soula, F-31400 Toulouse, France

[2]PSA Peugeot Citroën, Centre Technique de Velizy, 2 Route de Gisy, 78943 Vélizy-Villacoublay CEDEX, France

The steady, spanwise-periodic, symmetric (varicose) optimal blowing and suction that maximizes energy amplification in the circular cylinder wake is computed at Reynolds numbers ranging from 50 to 100. It is found that the cylinder wake can sustain large energy amplifications that are associated with the generation by the optimal blowing and suction of streamwise vortices near the cylinder, which then induce the transient spatial growth of high-energy streamwise streaks further downstream. The most amplified perturbations have spanwise wavelengths ranging from five to seven times the cylinder diameter at the Reynolds numbers considered, with the corresponding optimal streaks reaching their maximum amplitude in the near wake, inside the pocket of absolute instability which sustains the global instability. The optimal blowing and suction is shown to stabilize the global linear instability. The most stabilizing spanwise wavelengths are in good agreement with previous findings. The amplitude of optimal blowing and suction required to suppress the global instability decreases when the Reynolds number Re is increased from 75 to 100. This trend reveals the key role played by the non-normal amplification of the streaks in the stabilization process, which is able to overcome the increase of the uncontrolled global growth rate with Re. Finally, it is shown that the global instability can be suppressed with control amplitudes smaller than those required by 2-D (spanwise-uniform) control. This result is not what would be expected from first-order sensitivity analyses, which predict a zero sensitivity of the global instability to spanwise-periodic control and, in general, a non-zero sensitivity to spanwise-uniform control.

Key words: absolute/convective instability, instability control, wakes/jets

1. Introduction

There is continuing interest in the control of self-sustained oscillations in bluff-body wakes, the archetype of which is the circular cylinder wake. The steady flow around a circular cylinder undergoes a Hopf bifurcation at Reynolds number $Re \approx 48$, leading to robust periodic self-sustained oscillations in the wake associated with the shedding

† Email address for correspondence: carlo.cossu@imft.fr

of two-dimensional (spanwise-uniform) von Kármán vortices. The Hopf bifurcation occurs in correspondence to a linear global instability driven by a pocket of local absolute instability in the near wake (Chomaz, Huerre & Redekopp 1988; Monkewitz 1988). Different approaches to suppressing these self-sustained oscillations have been studied, which can be classified into 2-D (spanwise-uniform) and 3-D (typically spanwise-periodic) control (Choi, Jeon & Kim 2008). Examples of 3-D control were given by Tanner (1972), Tombazis & Bearman (1997), Bearman & Owen (1998) and Darekar & Sherwin (2001), among others, who have shown that suitable spanwise-periodic modulations of the bluff-body geometry weaken and can even suppress the vortex shedding in the wake. Kim & Choi (2005) obtained similar results using spanwise-periodic blowing and suction (the reader is referred to the article by Choi *et al.* 2008 for a complete review of these results).

In addition to early interpretations of the stabilizing effect of 3-D control on 2-D wakes in terms of vortex dynamics, arguments based on general linear stability concepts have been advanced recently. In particular, it has been shown by Hwang, Kim & Choi (2013) that the local absolute growth rate of standard wake profiles can be reduced with suitable spanwise-periodic modulations of the streamwise velocity. This stabilizing effect is observed for shapes and spanwise wavelengths which are in agreement with previous observations.

A mathematically similar, but physically different, application of 3-D control is encountered in boundary layers where the 3-D spanwise-periodic modulations of the streamwise velocity are called ‘streamwise streaks’. Kachanov & Tararykin (1987) found that streamwise streaks have a stabilizing effect on the primary 2-D instability of the flat-plate boundary layer. In the context of wall-bounded shear flows, it is well known that a very efficient way to generate streamwise streaks is to force low-energy streamwise vortices that fuel the growth of the streamwise streaks through the lift-up effect (see Moffatt 1967; Ellingsen & Palm 1975; Landahl 1990). In this process the energy of the vortices can be amplified by a factor proportional to Re^2 to give high-energy streaks (Gustavsson 1991). The precise shape of optimal vortices leading to optimally amplified streaks can be computed using standard optimization techniques and is associated with very large energy amplifications. Cossu & Brandt (2002, 2004) proposed using optimal vortices to force the stabilizing streaks, and showed that the primary 2-D instability of flat-plate boundary layers can be strongly stabilized in this way. The experiments of Fransson *et al.* (2006) show that transition to turbulence can be delayed by using this 3-D control technique.

Seeking to extend the approach used for boundary layers to bluff-body wakes, we recently computed the optimal streamwise uniform perturbations sustained by parallel absolutely unstable wakes (Del Guercio, Cossu & Pujals 2014*a*) and showed that, also in wakes, the optimal input consists of streamwise vortices and the optimal output consists of greatly amplified streamwise streaks. These optimally amplified streaks were shown to reduce the absolute growth rate and for sufficiently large amplitudes to completely suppress it, suggesting that global instabilities could be suppressed by quenching the wave-maker region in the near wake. To confirm this intuition, non-parallel model wakes with a finite region of absolute instability have been considered in a follow-up study (Del Guercio, Cossu & Pujals 2014*b*). Optimal downstream energy amplifications of steady perturbations were computed for these model wakes. It was found that inlet steady vortices (the control) can give rise to greatly amplified streaks downstream and that these streaks have a stabilizing effect on the global instability, leading to its suppression with sufficiently large control amplitudes.

By considering idealized non-parallel model wakes (as done in Del Guercio *et al.* 2014*b*), it is possible to analyse the streak generation and the global instability control

independently of the specific body generating the wake. However, this approach does not address the issue of how optimal steady vortices can be forced in practical applications. Some interesting questions therefore remain unanswered. Can large spatial energy amplifications be obtained by using a control device placed on the cylinder surface at low Reynolds numbers, e.g. ranging from 50 to 100? How do these optimal amplifications relate to those obtained for the idealized non-parallel wake? Does an optimally amplified finite spanwise wavelength exist in this case? If so, what is its value and how does this value compare to spanwise wavelengths that minimize the control energy? What is the minimum energy required to stabilize the global instability at Reynolds numbers ranging from, e.g., 50 to 100? How does the distribution of optimal blowing and suction compare with distributions used in previous investigations? How much can the control energy be reduced by using optimal forcing?

Another issue which has been addressed only partially by previous investigations is the comparative efficiency of spanwise-uniform (2-D) and spanwise-periodic (3-D) control for stabilization of the global instability. Hwang *et al.* (2013) had shown that the sensitivity of the absolute growth rate of parallel wakes to 3-D modulations of the basic flow is zero, whereas it is in general not zero for 2-D modulations. They therefore suggested that the higher efficiency of 3-D control, as observed by Kim & Choi (2005), for example, should be attributed to the higher efficiency of the forcing of 3-D perturbations as compared to 2-D ones. Del Guercio *et al.* (2014*b*) extended these sensitivity analysis results to global instabilities, showing that the first-order sensitivity of the global growth rate to 3-D modulations of the basic flow is also zero. They found that, despite this prediction, optimal 3-D perturbations are more efficient than 2-D ones in reducing the global growth rate in terms of both control energy and streak amplitude. It is currently unknown whether these conclusions can be extended to 'real' highly non-parallel wakes where the streaks would be forced by perturbations applied to the bluff-body surface.

The present study aims to answer the questions discussed above. To this end, we compute the optimal spanwise-periodic distributions of steady blowing and suction applied to the cylinder surface which maximize the perturbation energy at selected downstream stations. This approach is different from those where optimal initial or inflow conditions leading to the optimal temporal energy amplification are sought (see, e.g., Abdessemed *et al.* 2009 for the specific case of the circular cylinder). As detailed in § 2.1, the 3-D optimal blowing and suction and the associated optimal streaks are computed using a subspace reduction technique based on a set of independent simulations of the linearized Navier–Stokes equations. The results of the optimization, as well as their dependence on the spanwise wavelength and the Reynolds number, are discussed in § 3. The effect of finite-amplitude optimal blowing and suction on the growth rate of the unstable global mode is analysed in § 4. To this end, streaky wake basic flows are first computed by using finite-amplitude optimal forcing in nonlinear simulations; then, their linear stability is assessed by integration of the Navier–Stokes equations linearized near these streaky basic flows. The control sensitivity and efficiency are also discussed in § 4. Finally, nonlinear simulations are performed to validate the results of the linear stability analysis, as reported in § 4.6. The results and their implications are discussed in § 5.

2. Problem formulation

2.1. *Mathematical formulation*

We consider the flow of an incompressible viscous fluid of density ρ and kinematic viscosity ν past a circular cylinder of diameter D whose z axis is orthogonal to the

free-stream velocity $U_\infty \boldsymbol{e}_x$ (where $\boldsymbol{e}_x$ is the unit vector oriented parallel to the x axis). The Navier–Stokes equations governing the flow read as follows:

$$\boldsymbol{\nabla} \cdot \boldsymbol{u} = 0, \tag{2.1}$$

$$\frac{\partial \boldsymbol{u}}{\partial t} + \boldsymbol{u} \cdot \boldsymbol{\nabla} \boldsymbol{u} = -\boldsymbol{\nabla} p + \frac{1}{Re} \nabla^2 \boldsymbol{u}, \tag{2.2}$$

where $\boldsymbol{u}$ and p and the dimensionless velocity and pressure fields and $Re = U_\infty D/\nu$ is the Reynolds number. The velocity, pressure, lengths and times have been made dimensionless with U_∞, ρU_∞^2, D and D/U_∞, respectively. On the cylinder surface we enforce a radial velocity distribution $\boldsymbol{u}_w = \boldsymbol{u}(r = 1/2, \theta, z) = u_w(\theta, z)\boldsymbol{e}_r$, where $\boldsymbol{e}_r$ is the radial unit vector.

The reference basic flow $\boldsymbol{U}_{2D}(x, y)$ is obtained as a steady solution of the Navier–Stokes equations (2.1) and (2.2) in the case where no velocity is forced on the cylinder surface ($\boldsymbol{u}_w = \boldsymbol{0}$); $\boldsymbol{U}_{2D} = U(x, y)\boldsymbol{e}_x + V(x, y)\boldsymbol{e}_y$ is invariant with respect to translations and reflections in the spanwise coordinate z and is therefore two-dimensional (2-D).

In the first part of our study, which deals with linear optimal spatial perturbations of $\boldsymbol{U}_{2D}$, we consider steady perturbations $\boldsymbol{u}'$ of $\boldsymbol{U}_{2D}$ obtained by forcing a steady small radial velocity distribution $u'_w(\theta, z)\boldsymbol{e}_r$ on the cylinder surface. These perturbations satisfy the Navier–Stokes equations rewritten in perturbation form, i.e.

$$\boldsymbol{\nabla} \cdot \boldsymbol{u}' = 0, \tag{2.3}$$

$$\frac{\partial \boldsymbol{u}'}{\partial t} + \boldsymbol{u}' \cdot \boldsymbol{\nabla} \boldsymbol{U} + \boldsymbol{U} \cdot \boldsymbol{\nabla} \boldsymbol{u}' + \boldsymbol{u}' \cdot \boldsymbol{\nabla} \boldsymbol{u}' = -\boldsymbol{\nabla} p' + \frac{1}{Re} \nabla^2 \boldsymbol{u}', \tag{2.4}$$

using $\boldsymbol{U} = \boldsymbol{U}_{2D}$ as the basic flow and neglecting the nonlinear term $\boldsymbol{u}' \cdot \boldsymbol{\nabla} \boldsymbol{u}'$, which makes the perturbation equations linear. In the following, we will consider steady, spanwise-periodic perturbations of wavelength λ_z, which are of particular interest in open-loop flow control applications.

The (input) kinetic energy density per spanwise wavelength of the radial flow forced at the cylinder boundary is, in dimensionless form,

$$e'_w = \frac{1}{2\pi\lambda_z} \int_0^{\lambda_z} \int_0^{2\pi} (u'_w)^2 \, \mathrm{d}\theta \, \mathrm{d}z, \tag{2.5}$$

while the (output) local perturbation kinetic energy density at the station is

$$e'(x) = \frac{1}{\pi\lambda_z} \int_{-\infty}^{\infty} \int_0^{\lambda_z} \boldsymbol{u}' \cdot \boldsymbol{u}' \, \mathrm{d}y \, \mathrm{d}z. \tag{2.6}$$

The optimal spatial energy amplification of wall-control forcing is

$$G(x) = \max_{u_w} \frac{e'(x)}{e'_w}. \tag{2.7}$$

To compute $G(x)$ and the associated optimal wall perturbation, we follow an approach similar to the one recently applied to synthetic non-parallel wakes (Del Guercio *et al.* 2014*b*), which is summarized below. The control radial velocity enforced at the cylinder surface $u'_w(\theta, z)$ is decomposed using a set of linearly independent functions $b_w^{(m)}$, in practice limited to M terms, as

$$u'_w(\theta, z) = \sum_{m=1}^{M} q_m b_w^{(m)}(\theta, z). \tag{2.8}$$

If the perturbation velocity field obtained using $b_w^{(m)}(\theta, z)$ as the input perturbation is denoted by $\boldsymbol{b}^{(m)}(x, y, z)$, from linearity it follows that

$$\boldsymbol{u}'(x, y, z) = \sum_{m=1}^{M} q_m \boldsymbol{b}^{(m)}(x, y, z), \tag{2.9}$$

where the coefficients q_m are the same ones as in (2.8). The optimal energy growth, defined in (2.7), can therefore be approximated by

$$G(x) = \max_{\boldsymbol{q}} \frac{\boldsymbol{q}^{\mathrm{T}} \boldsymbol{H}(x) \boldsymbol{q}}{\boldsymbol{q}^{\mathrm{T}} \boldsymbol{H}_w \boldsymbol{q}}, \tag{2.10}$$

where $\boldsymbol{q}$ is the M-dimensional control vector and the components of the symmetric matrices $\boldsymbol{H}(x)$ and $\boldsymbol{H}_w$ are

$$H_{mn}(x) = \frac{1}{\pi \lambda_z} \int_{-\infty}^{\infty} \int_{0}^{\lambda_z} \boldsymbol{b}^{(m)}(x, y, z) \cdot \boldsymbol{b}^{(n)}(x, y, z)\, \mathrm{d}y\, \mathrm{d}z, \tag{2.11}$$

$$H_{w,mn} = \frac{1}{2\pi \lambda_z} \int_{0}^{\lambda_z} \int_{0}^{2\pi} b_w^{(m)}(\theta, z)\, b_w^{(n)}(\theta, z)\, \mathrm{d}\theta\, \mathrm{d}z. \tag{2.12}$$

The $G(x)$ in (2.10) is easily found as the largest eigenvalue μ_{max} of the generalized $M \times M$ eigenvalue problem $\mu \boldsymbol{H}_w \boldsymbol{w} = \boldsymbol{H} \boldsymbol{w}$. The corresponding eigenvector $\boldsymbol{q}^{(opt)}$ is the set of optimal coefficients maximizing the kinetic energy amplification at the selected streamwise station x, and the corresponding optimal blowing and suction is given by $u_w'^{(opt)}(\theta, z) = \sum_{m=1}^{M} q_m^{(opt)} b_w^{(m)}(\theta, z)$. The maximum growth is then defined as $G_{max} = \max_x G(x)$.

In the second part of the study, the effect of forcing three-dimensional finite-amplitude optimal perturbations on the global stability is investigated. To this end, first a set of increasingly three-dimensional basic flows $\boldsymbol{U}_{3D}(x, y, z; A_w)$ is obtained by computing steady solutions of the nonlinear Navier–Stokes equations with boundary conditions $\boldsymbol{u}_w = A_w u_w'^{(opt)}(\theta, z)\, \boldsymbol{e}_r$ (where $u_w'^{(opt)}$ is normalized to unit energy so that $e_w' = A_w^2$). The global linear stability of the $\boldsymbol{U}_{3D}$ basic flows is then analysed by integrating in time the linearized form of the Navier–Stokes equations (2.3) and (2.4) with $\boldsymbol{U} = \boldsymbol{U}_{3D}$ and enforcing $\boldsymbol{u}_w' = \boldsymbol{0}$. For sufficiently large times, the leading global mode emerges, inducing an exponential growth or decay of the solution. In this regime, the global growth rate is deduced from the slope of the global energy amplification curve.

2.2. *Numerical methods*

Numerical simulations of both the nonlinear and the linearized Navier–Stokes equations were performed using OpenFoam, an open-source finite volume code (see http://www.openfoam.org). The flow is solved in a C-type domain centred on the cylinder with L_x streamwise, L_y transverse and L_z spanwise extensions (see figure 1). Several preliminary tests guided us to the choices $L_x = 70$ and $L_y = 80$, with $L_z = \lambda_z$ for the computation of optimal perturbations and nonlinear streaky wakes and $L_z = 2\lambda_z$ for the global stability analyses and nonlinear direct numerical simulations used to confirm that the control is effective. The grid density is increased in the x–y plane in regions of high shear. We used $N_x = 300$ and $N_y = 200$ points in the streamwise and transverse directions, respectively, with $\Delta x_{min} = 0.01$, $\Delta x_{max} = 0.2$, $\Delta y_{min} = 0.01$ and $\Delta y_{max} = 0.2$ in the internal mesh blocks. A uniform grid spacing was used in the spanwise direction, always with $\Delta z \approx 0.25$, and the number of points used with each L_z is summarized in table 1. The PISO (Pressure Implicit with Splitting of

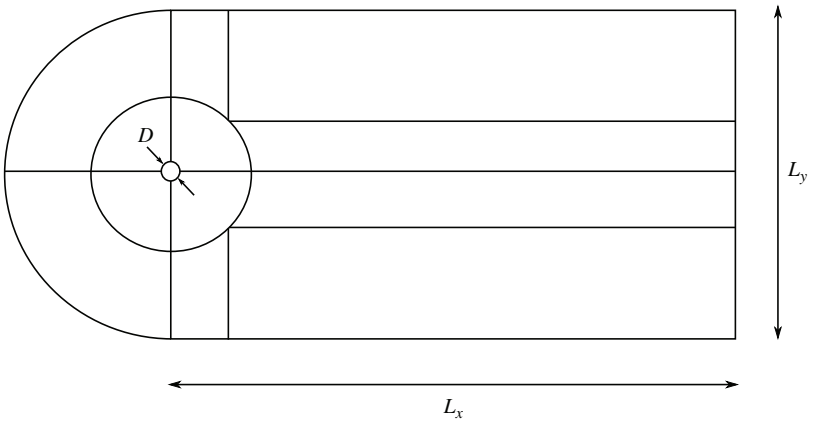

FIGURE 1. Numerical solution domain. For clarity, only the boundaries of the mesh blocks are shown.

L_z	12.57	8.37	6.28	5.03	4.20	3.60	3.14
N_z	48	34	24	20	16	14	12

TABLE 1. Spanwise extension L_z of the solution domain and the number of points N_z used in the spanwise direction for computation of the basic flows and optimal perturbations; L_z and N_z are doubled for the global stability analysis and for the nonlinear simulations.

Operators) algorithm is used to advance the solution in time. We have verified that with the chosen mesh, the length of the recirculation region of steady symmetric solutions and the drag coefficient both match, within 1 % accuracy, those found by Kim & Choi (2005) and Giannetti & Luchini (2007) in the 2-D case for the range of Reynolds numbers considered. Extending the domain size in the streamwise direction to $L_x = 100$ or in the transverse direction to $L_y = 100$ does not significantly improve the precision of these results. For 3-D simulations we have verified, in a few selected cases with active blowing and suction, that the perturbation energy (from which global growth rates are computed) does not change by more than 1 % when the number of grid points is doubled in the spanwise direction.

3. Optimal spatial energy amplifications sustained by the 2-D wake

The 2-D cylinder wake steady solution $\boldsymbol{U}_{2D}$ is the usual one computed in a number of previous studies (see, e.g., Dennis & Chang 1970; Fornberg 1980). It is found that $\boldsymbol{U}_{2D}$ is stable for $Re < Re_c \approx 48$. Here, $\boldsymbol{U}_{2D}$ is computed in the linearly unstable regime, for $Re = 50$, 75 and 100, by enforcing the y-symmetry of the solutions in direct temporal integrations of the Navier–Stokes equations. We have verified that the length of the recirculation bubble and the value of the separation angle are in good agreement with those found in previous studies.

Distributions of optimal blowing and suction $u_w(\theta, z)$ which maximize the spatial amplification of perturbation energy are computed following the procedure described in § 2.1. As the basic flow $\boldsymbol{U}_{2D}$ is spanwise invariant and the equations are linear, single-harmonic spanwise-periodic perturbations can be considered without loss of generality, i.e. $u'_w(\theta, z) = f(\theta)\sin(2\pi z/\lambda_z)$. A number of previous studies have shown

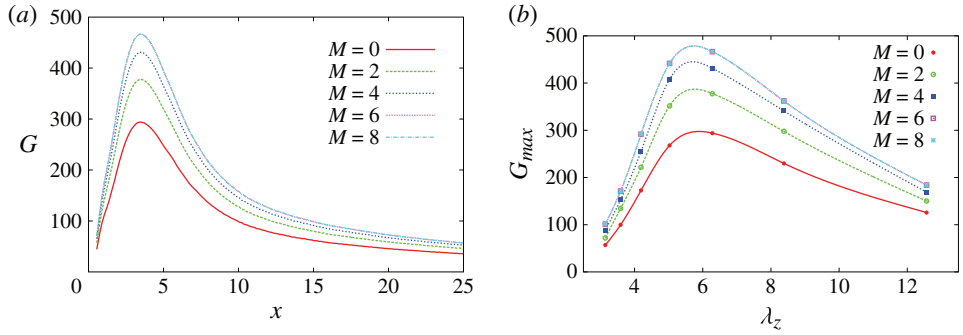

FIGURE 2. (Colour online) Convergence at $Re = 75$ of (a) the optimal energy growth $G(x)$ for $\lambda_z = 2\pi$ and (b) $G_{max}(\lambda_z)$, as the number M of linearly independent distributions of wall blowing and suction is increased. Well-converged results are obtained with $M = 6$.

that varicose perturbations (which are mirror-symmetric with respect to the $y = 0$ plane) are the most efficient for control (see, e.g., Darekar & Sherwin 2001; Kim & Choi 2005; Choi *et al.* 2008; Hwang *et al.* 2013; Del Guercio *et al.* 2014*a*,*b*), even if they are slightly less amplified than sinuous ones (Del Guercio *et al.* 2014*a*). We therefore enforce $f(-\theta) = f(\theta)$, which leads to varicose streaks. A standard cosine series expansion in θ is used, leading to the choice $b_w^{(m)}(\theta, z) = \cos(m\theta)\sin(2\pi z/\lambda_z)$ $(m = 0, \ldots, M)$ for the set of linearly independent inflow conditions used in (2.8). Optimal energy growths have been computed by increasing M until a precision of 1 % or better on G_{max} was achieved for a set of spanwise wavelengths λ_z. Typical $G(x)$ and $G_{max}(\lambda_z)$ obtained for $Re = 75$, along with their convergence histories, are reported in figure 2. From the figure one can see that the optimal growths have converged with better than 1 % precision with only $M = 6$ terms.

The computations have been repeated at $Re = 50$ and 100. The convergence of the results with increasing M is similar to that in the $Re = 75$ case. As shown in figure 3, the main effect of an increase in Re is to increase both the maximum amplification G_{max} and the position x_{max} at which this maximum is attained. The large amplifications found are consistent with those found in our previous investigations (Del Guercio *et al.* 2014*a*,*b*) and with those of Abdessemed *et al.* (2009), who found optimal temporal energy amplifications of the order of 10–10^2 for initial perturbations with $4 \lesssim \lambda_z \lesssim 8$ at $Re = 45$. From figure 3(b) it is also seen that x_{max} is an increasing function of λ_z. The most amplified wavelengths are found to be $\lambda_z = 6.5$ for $Re = 50$, $\lambda_z = 5.7$ for $Re = 75$ and $\lambda_z = 6.1$ for $Re = 100$, with corresponding optimal streamwise stations $x_{max} = 3.4$, $x_{max} = 3.5$ and $x_{max} = 3.6$.

The radial distributions $\widetilde{u}_w^{(opt)}(\theta)$ of the optimal blowing and suction $\widetilde{u}_w^{(opt)}(\theta) \times \sin(2\pi z/\lambda_z)$ are shown in figure 4. They correspond to spanwise-periodic blowing and suction with a maximum near $\theta \approx \pm 90°$ and minima at the bow and the stern of the cylinder. The variations of $\widetilde{u}_w^{(opt)}(\theta)$ with λ_z and Re are small and may be neglected in a first approximation. As shown in figure 5, this spanwise-periodic optimal blowing and suction induces counter-rotating streamwise vortices which decay downstream while forcing the growth of varicose streamwise streaks. Also in this relatively complicated flow, therefore, the main mechanism at play seems to be the lift-up effect. The facts that $\widetilde{u}_w^{(opt)}(\theta)$ is maximal at $\theta \approx \pm 90°$ (and not at, e.g., $\theta = 0$ and $\theta = 180°$) and that the local (in z) net mass flux is not zero (the $M = 0$ harmonic has an important contribution) suggest that the main effect of the optimal

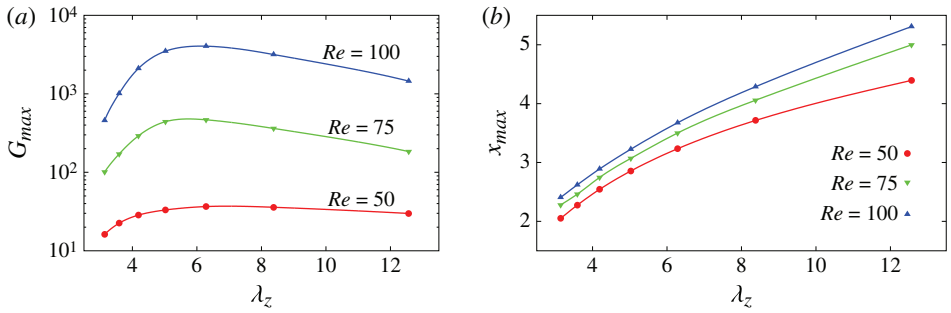

FIGURE 3. (Colour online) Dependence on the spanwise wavelength λ_z of (a) the maximum transient energy growth G_{max} and (b) the streamwise station x_{max} at which the maximum is attained, for selected Reynolds numbers $Re = 50$, 75 and 100.

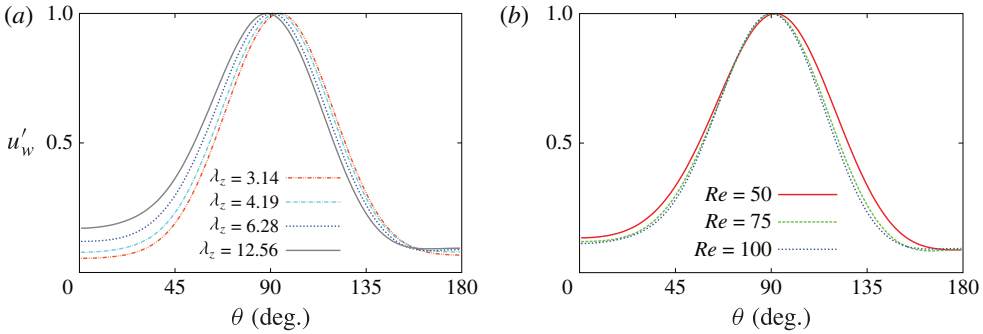

FIGURE 4. (Colour online) Azimuthal distributions $\widetilde{u}_w^{(opt)}(\theta)$ of the optimal blowing and suction normalized by their maximum value: (a) results obtained for a set of spanwise wavelengths λ_z at $Re = 75$; (b) distributions pertaining to the most amplified λ_z at each considered Reynolds number.

blowing and suction is to force the streamwise vortices that will best exploit the lift-up effect.

The existence of a finite optimal value of λ_z is probably the most important difference from our previous results pertaining to parallel and non-parallel synthetic wakes, where G_{max} was a monotonic increasing function of λ_z (Del Guercio *et al.* 2014*a*,*b*). This difference is due to the fact that in those previous investigations the optimal perturbations could assume any admissible shape in y, and indeed their y-extension increased with λ_z. In the present case, because the velocity forcing is localized on the cylinder surface, only a finite effective extension in y can be efficiently attained, and therefore a maximum value of G_{max} is attained in correspondence to the λ_z values for which the effective maximum y-extension of the forced functions is reached.

Finally, it is instructive to compare the effects of the optimal distribution of blowing and suction here and the θ-localized one used by Kim & Choi (2005). Simulations of the linearized Navier–Stokes equations show that the maximum energy gain attained with localized blowing and suction located at $\theta = 90°$ is 75 times smaller than the maximum energy gain obtained by using optimal blowing and suction. The two gain curves are, however, nearly indistinguishable if renormalized by the maximum gain

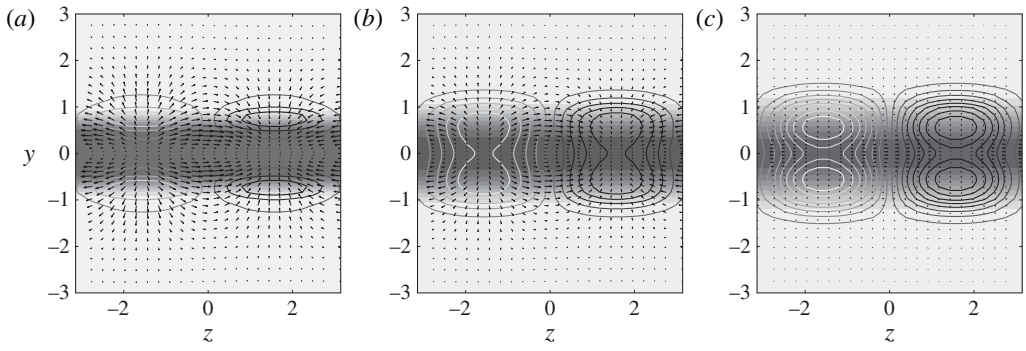

FIGURE 5. Cross-stream (y–z) view of the velocity perturbations forced by the optimal blowing and suction at $Re = 75$ with $\lambda_z = 2\pi$ at three selected streamwise stations: (a) $x = 1/2$ (cylinder stern); (b) $x = x_{max}/2$ (midway to the position of maximum streak amplitude); (c) $x = x_{max}$ (position of maximum streak amplitude). The scale used to plot the streamwise u' (streamwise streaks, contour lines) and the cross-stream v'–w' components (streamwise vortices, arrows) is the same in all panels. The reference 2-D basic flow streamwise velocity $U_{2D}(y)$ is represented in grey-scale with light grey corresponding to the freestream velocity and dark grey corresponding to the minimum velocity (wake centreline).

(not shown), meaning that streaks with essentially the same shape are forced. The main effect of using optimal perturbations is therefore to reduce the input energy for forcing these streaks.

4. Stabilizing effect of finite-amplitude optimal streaks

4.1. *A family of steady nonlinear streaky wake basic flows*

Non-parallel streaky (3-D) wake basic flows $\boldsymbol{U}_{3D}(x, y, z; A_w)$ are computed by enforcing at the wall the boundary condition $U_w(\theta, z) = A_w u_w'^{(opt)}(\theta, z)$ and then computing the corresponding steady solution of the nonlinear Navier–Stokes equations, as explained in § 2.1. Symmetry with respect to the $y = 0$ plane is enforced to compute steady solutions which may be unstable. A few cases with increasing A_w are selected and listed in table 2. We consider the intermediate Reynolds number $Re = 75$ and the spanwise wavelength $\lambda_z = 2\pi$, which is chosen slightly ($\approx$10 %) larger than its optimal value 5.7 so as to approach the value that minimizes the control energy, as discussed below.

The reference two-dimensional wake profile $\boldsymbol{U}_{2D}$ is called case A, and cases B, C and D correspond to increasingly streaky wakes, as shown in figure 6. The local streak amplitude is measured with the standard formula of Andersson *et al.* (2001),

$$A_s(x) = \frac{\max_{y,z}(U_{3D} - U_{2D}) - \min_{y,z}(U_{3D} - U_{2D})}{2U_\infty}. \tag{4.1}$$

The evolutions $A_s(x)$ associated with the velocity fields $\boldsymbol{U}_{3D}$ corresponding to the four cases are plotted in figure 7(a), and the corresponding maximum streak amplitudes $A_{s,max}$ are listed in table 2. It is interesting that the maximum streak amplitudes are naturally reached inside the region of absolute instability of the reference 2-D wake, which almost coincides with the recirculation region ($x \lesssim 5$ at $Re = 75$). This is good news. Indeed, the global instability has been shown to be sustained by the region

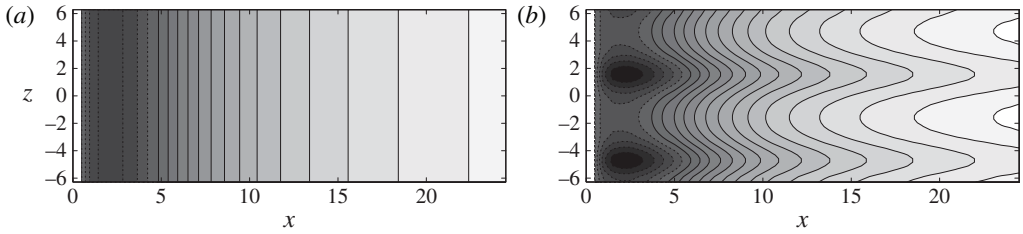

FIGURE 6. Distribution of the streamwise velocity $U_{3D}(x, y=0, z)$ in the $y=0$ symmetry plane of two selected basic flows: (a) the reference 2-D case, i.e. case A; (b) the streaky wake of case C. Contour levels are spaced by $u_\infty/20$, with low (high) velocities represented by dark (light) grey.

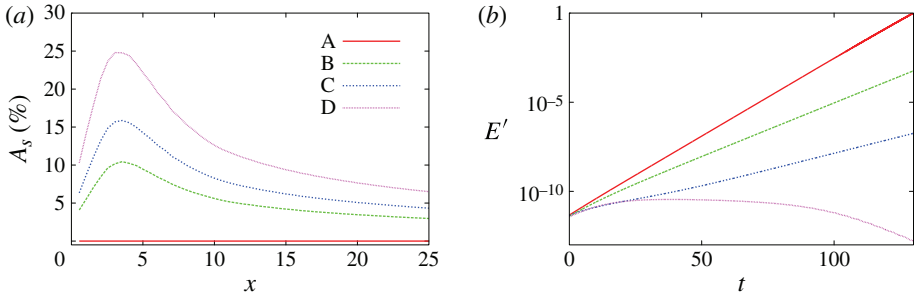

FIGURE 7. (Colour online) Plots for increasing amplitudes A_w of the optimal blowing and suction: (a) spatial evolution of the nonlinear streak amplitude $A_s(x)$; (b) temporal evolution of the global kinetic energy density $E'(t)$ of secondary perturbations to the nonlinear basic flows under consideration. The results were obtained for $Re = 75$ and $\lambda_z = 2\pi$.

Case	A	B	C	D
A_w	0	0.0031	0.0048	0.0080
$u_{w,max}$ (%)	0	0.75	1.2	2.1
$A_{s,max}$ (%)	0	10.45	16.16	25.44

TABLE 2. Nonlinear streaky wakes considered in this study: A_w is the finite amplitude of the optimal blowing and suction corresponding to the root-mean-square (r.m.s.) value of the blowing or suction velocity; $u_{w,max}$ is the maximum absolute value of the blowing or suction velocity; $A_{s,max}$ is the maximum streak amplitude reached in the wake. Values of $A_{s,max}$ and $u_{w,max}$ are given as percentages of U_∞. Case A corresponds to the reference 2-D wake, while cases B, C and D are for increasing values of A_w and correspond to increasingly streaky wakes. All the data refer to the parameter settings $Re = 75$ and $\lambda_z = 2\pi$.

of absolute instability, which acts as a wave-maker (see, e.g., Huerre & Monkewitz 1990); this is therefore the region where it is useful to reduce the absolute growth rate. As this reduction is proportional to the square of the streak amplitude, as shown by Hwang *et al.* (2013) and Del Guercio *et al.* (2014*a*), having large-amplitude streaks in the wave-maker region is therefore expected to induce a high control efficiency.

4.2. *Global linear stability of the streaky wakes*

The global linear stability of the nonlinear streaky basic flows is examined by integrating with respect to time the Navier–Stokes equations (2.3) and (2.4), linearized with respect to the $\boldsymbol{U}_{3D}$ considered. The linearized equations are integrated over a domain including two basic flow streak spanwise wavelengths ($L_z = 2\lambda_z$) to take into account the potential subharmonic nature of the dominant absolute mode (see Hwang *et al.* 2013; Del Guercio *et al.* 2014*a*,*b*). For the reference 2-D wake (case A), a random solenoidal perturbation velocity field $\boldsymbol{u}'$ is chosen as initial condition and the integration is continued in time until the emergence of the unstable global mode. This global mode is then renormalized to a small amplitude and used as the initial condition for all the cases under consideration. We then monitor the evolution of the global perturbation kinetic energy density $E' = (1/\mathscr{V}) \int_{\mathscr{V}} \boldsymbol{u}' \cdot \boldsymbol{u}' \, \mathrm{d}x \, \mathrm{d}y \, \mathrm{d}z$, where $\mathscr{V}$ is the fluid control volume. As shown in figure 7(*b*), $E'(t)$ grows exponentially in time, after the extinction of the initial transient. In this regime, the exponential growth rate of E' is twice that of the most unstable global mode. At the Reynolds number considered, $Re = 75$, it is already well known that the reference 2-D wake (case A) is linearly unstable. In the presence of increasing amplitudes of optimal blowing and suction and, therefore, increasing amplitudes of the streaks, the growth rate of the global mode is initially reduced (cases B and C), becoming negative for case D. These results confirm for a 'real wake' the scenario already observed in non-parallel model wakes (Del Guercio *et al.* 2014*b*) and associated with the weakening or complete suppression of the pocket of absolute instability, in accordance with the conclusions of Hwang *et al.* (2013) and Del Guercio *et al.* (2014*a*).

4.3. *Sensitivity of the global growth rate to the 3-D control amplitude*

Let us now examine the dependence of the growth rate s_r on the control amplitude at $Re = 75$, shown in figure 8 for a selected set of spanwise wavelengths. The amplitude of the control is reported in terms of both the optimal blowing and suction amplitude A_w and the maximum streak amplitude $A_{s,max}$. In all the computed cases, the data $s_r(A)$ are well approximated by the quadratic fit $s_r(Re, \lambda_z, A) = s_{r,2D}(Re) - C(Re, \lambda_z) A^2$, where $s_{r,2D}$ is the growth rate of the uncontrolled 2-D reference wake, A is the amplitude and C is a constant. Such a quadratic dependence is expected from first-order sensitivity analyses, which predict that for spanwise-periodic basic flow modulations, $\mathrm{d}s_r/\mathrm{d}A|_{A=0} = 0$ (see, e.g., Del Guercio *et al.* 2014*b* for the global mode sensitivity analysis). That the first-order sensitivity is zero could also have been inferred by observing that changing the sign of A in a spanwise-sinusoidal basic flow modification simply corresponds to a spanwise shift of $\lambda_z/2$ in physical space, and therefore we must have $s_r(A) = s_r(-A)$, implying a zero first-order derivative at the origin.

4.4. *Comparison of the control efficiency of 3-D and 2-D perturbations*

Since for 2-D modulations of the basic flow the first-order sensitivity is in general not zero (see, e.g., Bottaro, Corbett & Luchini 2003; Chomaz 2005), it might be

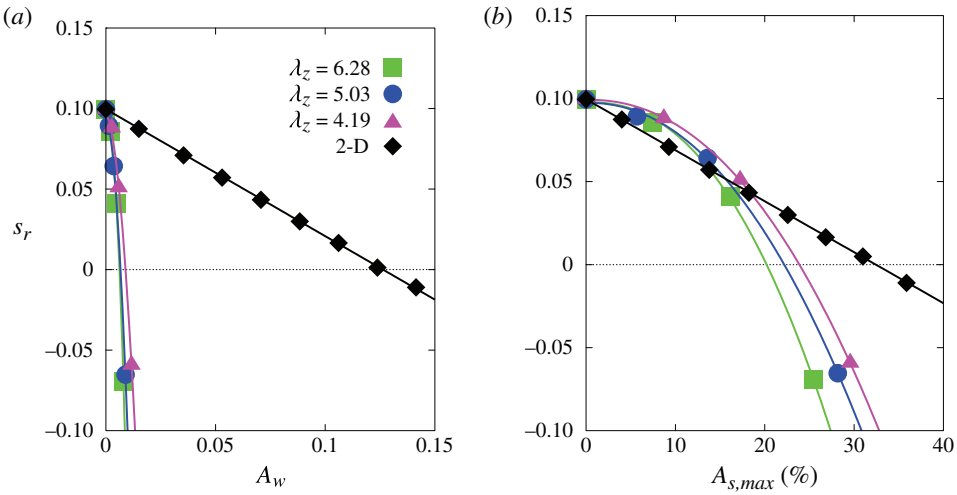

FIGURE 8. (Colour online) Dependence of the global mode growth rate s_r on (*a*) the optimal blowing and suction amplitude A_w and (*b*) the maximum streak amplitude $A_{s,max}$. A spanwise-uniform (2-D) perturbation has also been considered for comparison. The symbols represent data points, while the lines are best fits to the data points using quadratic interpolation for the 3-D data and linear interpolation for the 2-D data.

expected that 2-D perturbations are more effective than 3-D ones in quenching the global instability. To check whether this is actually the case, we computed the growth rate variations induced at $Re = 75$ by spanwise-uniform (2-D) wall blowing and suction with $m = 1$ azimuthal dependence $U_w = A_{2D}\cos(\theta)$, which has zero net mass flux and is associated with bleeding in the wake, and is known to efficiently reduce the absolute growth rate (Monkewitz 1988). The $s_{r,2D}(A_{2D})$ curves pertaining to the 2-D control are also plotted in figure 8 for comparison with the 3-D control. The analogue of the streak amplitude is defined for the 2-D perturbation as the maximum of the basic flow streamwise velocity variation induced by the 2-D suction.

As expected, the $s_{r,2D}(A_{2D})$ curve has non-zero slope at $A_{2D} = 0$ and is well approximated by a straight line. The 2-D perturbations considered are more stabilizing than the optimal 3-D ones only for $A_{s,max} \lesssim 14\,\%$, corresponding to the negligible $A_w \approx 0.005$. As already observed by Del Guercio *et al.* (2014*b*), a higher efficiency of 3-D perturbations is expected in terms of A_w, because such perturbations can exploit the energy gain associated with the lift-up effect, which is a 3-D mechanism. The fact that these 3-D perturbations are also more efficient in terms of basic flow deformation is not *a priori* obvious. We have verified that qualitatively similar results are obtained for a few other shapes of the 2-D forcing.

4.5. *Optimal spanwise wavelengths and amplitudes required for suppression of the global instability*

The dependence on the spanwise wavelength λ_z of the critical amplitudes A_c for which the global instability is suppressed is illustrated in figure 9 in terms of both A_w and $A_{s,max}$. At $Re = 75$, the spanwise wavelength minimizing the control amplitude necessary for the stabilization of the global instability is $\lambda_z \approx 6$. The value minimizing A_w ($\lambda_z = 6.2$) is slightly larger than that minimizing $A_{s,max}$ ($\lambda_z = 5.9$). When the

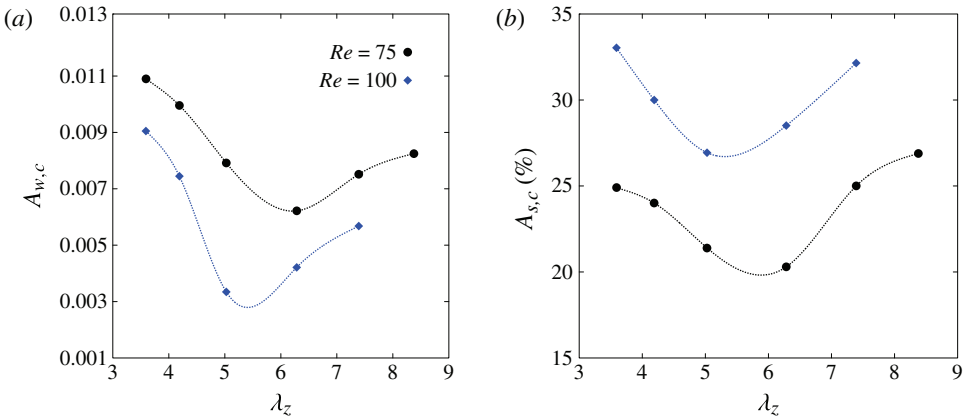

FIGURE 9. (Colour online) Dependence on the spanwise wavelength of (*a*) the critical amplitude of the forcing, $A_{w,c}$, and (*b*) the critical amplitude of the streaks, $A_{s,c}$, for which the global instability is suppressed. The data pertains to the Reynolds numbers $Re = 75$ and $Re = 100$.

Reynolds number is increased to $Re = 100$, the spanwise wavelength minimizing the control amplitude is reduced to $\lambda_z \approx 5.3$, with the value minimizing A_w ($\lambda_z = 5.4$) being very slightly larger than the one minimizing $A_{s,max}$ ($\lambda_z = 5.3$). These results are in very good agreement with those of Kim & Choi (2005), who found that the minimum drag is achieved for $\lambda_z = 5$–6 (but at the fastest rate for $\lambda_z = 6$) at $Re = 80$, and for $\lambda_z = 4$–5 (but at the fastest rate for $\lambda_z = 5$) at $Re = 100$. Less energy is required to suppress the global instability when using optimal blowing and suction instead of localized blowing and suction (0.62 % instead of 8 % of U_∞ in terms of maximum blowing/suction velocity, and 5.6×10^{-5} instead of 1.2×10^{-3} in terms of the momentum coefficient of forcing $C_\mu = 2\pi A_w^2$ at $Re = 100$), which is also confirmed by nonlinear simulations (not shown). This is not surprising given the observed large differences in energy gains obtained using these different distributions of blowing and suction. Despite its higher efficiency, however, the optimal distribution of blowing and suction may be more difficult to realize experimentally than localized blowing and suction.

For all the spanwise wavenumbers considered, larger streak amplitudes are required to stabilize the global instability at $Re = 100$ than at $Re = 75$. This is to be expected, because at $Re = 100$ the global mode is more unstable than at $Re = 50$, and hence larger streak amplitudes are needed to quench it. However, the amplitudes of the optimal blowing and suction required to stabilize the global instability are smaller at $Re = 100$ than at $Re = 75$, for all the λ_z considered. The increase in energy amplification of the control due to the lift-up associated with an increase in Reynolds number (see figure 3*a*) therefore overcomes the larger control action necessary to quench the more unstable global mode. In other words, the results reported in figure 9(*a*) confirm the essential role played by the non-normal amplification of streaks in stabilization of the global instability.

4.6. *Nonlinear simulations*

Finally, the stabilizing effect of optimal blowing and suction 3-D optimal perturbations is assessed in the fully nonlinear regime. The same cases examined with linear

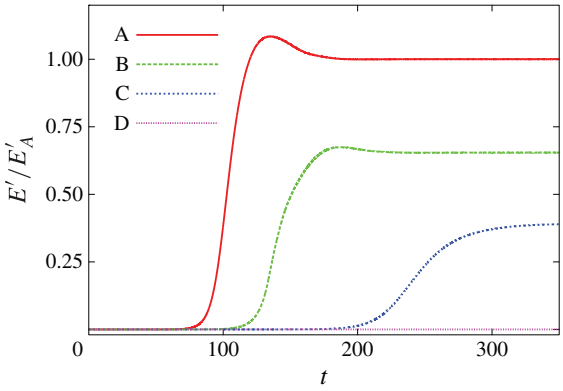

FIGURE 10. (Colour online) Temporal evolution of the normalized total perturbation kinetic energy density, $E'(t)/E'_A$, for increasing control amplitudes. The global perturbation kinetic energy $E'(t)$ is normalized with respect to the permanent regime value E'_A of the reference 2-D wake of case A. The results were obtained from fully nonlinear simulations at $Re = 75$ with $\lambda_z = 2\pi$.

simulations (see § 4.2) are re-examined by switching on the nonlinear terms in the numerical simulations and integrating the equations until a permanent regime develops. In all the cases considered, the permanent regime is periodic in time, except for sufficiently large amplitudes of the optimal blowing and suction, where, as expected from the linear analysis, self-sustained oscillations are quenched. Figure 10 shows that for increasing A_w, the mean value of the global perturbation kinetic energy E' in the permanent regime is reduced (cases B and C) and is eventually driven to zero for case D. The increasingly three-dimensional nature of the controlled wakes in the permanent regime can be appreciated from figure 11.

5. Summary and conclusions

In the first part of this study, a subspace reduction method was introduced for the computation of steady, spanwise-periodic, symmetric (varicose) optimal blowing and suction that maximizes the energy amplification at selected streamwise stations in the circular cylinder wake. It has been shown that the energy of the optimal blowing and suction can be greatly amplified in the wake and that the maximum energy amplification and the position at which it is reached are both increasing functions of the Reynolds number.

The azimuthal distribution of the optimal blowing and suction displays a maximum near $\theta = 90°$, in accordance with the results of Kim & Choi (2005), who found that the optimal position of θ-localized spanwise-periodic blowing and suction is near $\theta = 90°$. The optimal blowing and suction induces streamwise vortices, which in turn induce the transient spatial growth of highly amplified streamwise streaks. The most amplified spanwise wavelengths λ_z range from $5D$ to $7D$ at the Reynolds numbers considered, with the corresponding optimal streaks reaching their maximum amplitude at approximately $\lambda_z/2$ downstream in the wake, well inside the pocket of absolute instability sustaining the global instability. The existence of a finite optimal spanwise wavelength is one of the most notable differences between our results and the case of synthetic wakes studied by Del Guercio *et al.* (2014*b*), where the generation mechanism of the optimal vortices by actuation on the body surface was not taken into account.

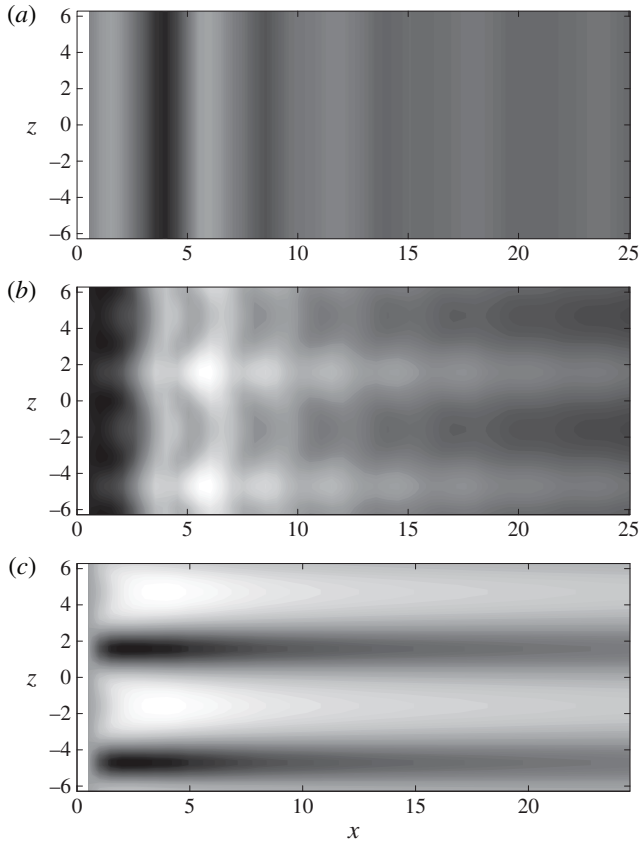

FIGURE 11. Streamwise perturbation velocity $u'(x, y=0, z) = u(x, y=0, z) - U_{2D}(x, y=0)$ in the $y=0$ symmetry plane in the permanent regime ($t=450$) of the fully nonlinear simulations at $Re=75$ for $\lambda_z = 2\pi$. (*a*) The reference 2-D case (case A) displays the usual self-sustained periodic oscillations of 2-D structures in the wake. (*b*) In the presence of moderate-amplitude 3-D perturbations (case C), the self-sustained periodic oscillations acquire a typical 3-D nature while reducing their r.m.s. amplitude. (*c*) For sufficiently large 3-D perturbations (case D), the periodic oscillations are completely suppressed and only the forced stable streaks are visible in the wake.

We then investigated the effect on the global linear instability of forcing optimal blowing and suction with finite amplitudes. First, nonlinear simulations were used to compute nonlinear streaky wake basic flows with increasing finite-amplitude optimal blowing and suction. Then, the global stability of these nonlinear streaky wakes was investigated using the linearized equations.

The global mode growth rate is shown to be reduced proportionally to the square of the optimal blowing and suction amplitude and to the square of the maximum amplitude of the associated streaks. Complete stabilization of the global mode is achieved with blowing and suction amplitudes much smaller than those required by 2-D (spanwise-uniform) blowing and suction. This result is not expected from first-order sensitivity analyses, which predict the opposite. Predictions based on first-order sensitivity analyses are therefore to be treated with extreme caution when considering spanwise-periodic controls and, more generally, when far from the

instability threshold. Indeed, higher-order terms are likely to become more important than linear terms when moderate control amplitudes are considered.

We also show that the optimal blowing and suction amplitude A_w required to suppress the global instability decreases when the Reynolds number is increased from 75 to 100, despite the fact that the global instability is stronger at $Re = 100$ than at $Re = 75$. This reveals the essential role played by the lift-up effect, which amplifies the control energy with an efficiency that increases with Re; this efficiency increase probably explains why 3-D control of 2-D wakes remains effective far from the critical Reynolds number, and even in the turbulent regime. The spanwise wavelength for which the stabilization is obtained with minimum amplitude is found to decrease from $\lambda_z \approx 6$ to $\lambda_z \approx 5$ as Re is increased from 75 to 100, in good agreement with the results of Kim & Choi (2005).

The present study also pinpoints the relevance of the role played by streamwise vortices in the very near wake. Indeed, although the analyses of Hwang *et al.* (2013) show that a key stabilizing role is played by the streaks, here and in our related previous investigations of parallel and non-parallel model wakes (Del Guercio *et al.* 2014*a*,*b*), we show that forcing optimal vortices instead of directly forcing the streaks is much more efficient and that the energy amplification associated with this process plays a key role in the stabilization. In this sense, the present results extend to 2-D wakes the rationale already implemented in boundary layers, where optimal or nearly optimal streamwise vortices were forced to induce streaks able to delay the 2-D Tollmien–Schlichting instability and delay transition to turbulence (Cossu & Brandt 2002, 2004; Fransson *et al.* 2005, 2006). Current effort is directed at extending the present approach to the control of turbulent wakes, in the same spirit as Cossu, Pujals & Depardon (2009), Pujals, Cossu & Depardon (2010*a*) and Pujals, Depardon & Cossu (2010*b*).

Acknowledgement

G.D.G. acknowledges the support of ANRT via the convention CIFRE 742/2011.

REFERENCES

Abdessemed, N., Sharma, A. S., Sherwin, S. J. & Theofilis, V. 2009 Transient growth analysis of the flow past a circular cylinder. *Phys. Fluids* **21**, 044103.

Andersson, P., Brandt, L., Bottaro, A. & Henningson, D. 2001 On the breakdown of boundary layer streaks. *J. Fluid Mech.* **428**, 29–60.

Bearman, P. W. & Owen, J. C. 1998 Reduction of bluff-body drag and suppression of vortex shedding by the introduction of wavy separation lines. *J. Fluids Struct.* **12** (1), 123–130.

Bottaro, A., Corbett, P. & Luchini, P. 2003 The effect of base flow variation on flow stability. *J. Fluid Mech.* **476**, 293–302.

Choi, H., Jeon, W. P. & Kim, J. 2008 Control of flow over a bluff body. *Annu. Rev. Fluid Mech.* **40**, 113–139.

Chomaz, J. M. 2005 Global instabilities in spatially developing flows: nonnormality and nonlinearity. *Annu. Rev. Fluid Mech.* **37**, 357–392.

Chomaz, J. M., Huerre, P. & Redekopp, L. G. 1988 Bifurcations to local and global modes in spatially developing flows. *Phys. Rev. Lett.* **60**, 25–28.

Cossu, C. & Brandt, L. 2002 Stabilization of Tollmien–Schlichting waves by finite amplitude optimal streaks in the Blasius boundary layer. *Phys. Fluids* **14**, L57–L60.

Cossu, C. & Brandt, L. 2004 On Tollmien–Schlichting waves in streaky boundary layers. *Eur. J. Mech. (B/Fluids)* **23**, 815–833.

COSSU, C., PUJALS, G. & DEPARDON, S. 2009 Optimal transient growth and very large scale structures in turbulent boundary layers. *J. Fluid Mech.* **619**, 79–94.

DAREKAR, R. M. & SHERWIN, S. J. 2001 Flow past a square-section cylinder with a wavy stagnation face. *J. Fluid Mech.* **426** (1), 263–295.

DENNIS, S. C. R. & CHANG, G. Z. 1970 Numerical solutions for steady flow past a circular cylinder at Reynolds numbers up to 100. *J. Fluid Mech.* **42**, 471–489.

ELLINGSEN, T. & PALM, E. 1975 Stability of linear flow. *Phys. Fluids* **18**, 487–488.

FORNBERG, B. 1980 A numerical study of steady viscous flow past a circular cylinder. *J. Fluid Mech.* **98**, 819–855.

FRANSSON, J., BRANDT, L., TALAMELLI, A. & COSSU, C. 2005 Experimental study of the stabilisation of Tollmien–Schlichting waves by finite amplitude streaks. *Phys. Fluids* **17**, 054110.

FRANSSON, J., TALAMELLI, A., BRANDT, L. & COSSU, C. 2006 Delaying transition to turbulence by a passive mechanism. *Phys. Rev. Lett.* **96**, 064501.

GIANNETTI, F. & LUCHINI, P. 2007 Structural sensitivity of the first instability of the cylinder wake. *J. Fluid Mech.* **581**, 167–197.

DEL GUERCIO, G., COSSU, C. & PUJALS, G. 2014*a* Stabilizing effect of optimally amplified streaks in parallel wakes. *J. Fluid Mech.* **739**, 37–56.

DEL GUERCIO, G., COSSU, C. & PUJALS, G. 2014*b* Optimal perturbations of non-parallel wakes and their stabilizing effect on the global instability. *Phys. Fluids* **26**, 024110.

GUSTAVSSON, L. H. 1991 Energy growth of three-dimensional disturbances in plane Poiseuille flow. *J. Fluid Mech.* **224**, 241–260.

HUERRE, P. & MONKEWITZ, P. A. 1990 Local and global instabilities in spatially developing flows. *Annu. Rev. Fluid Mech.* **22**, 473–537.

HWANG, Y., KIM, J. & CHOI, H. 2013 Stabilization of absolute instability in spanwise wavy two-dimensional wakes. *J. Fluid Mech.* **727**, 346–378.

KACHANOV, Y. S. & TARARYKIN, O. I. 1987 Experimental investigation of a relaxing boundary layer. *Izv. Sib. Otd. An. Tech.* **18**, 9–19.

KIM, J. & CHOI, H. 2005 Distributed forcing of flow over a circular cylinder. *Phys. Fluids* **17**, 033103.

LANDAHL, M. T. 1990 On sublayer streaks. *J. Fluid Mech.* **212**, 593–614.

MOFFATT, H. K. 1967 The interaction of turbulence with strong wind shear. In *Proceedings of the URSI-IUGG International Colloquium on Atmospheric Turbulence and Radio Wave Propagation* (ed. A. M. Yaglom & V. I. Tatarsky), pp. 139–154. Nauka.

MONKEWITZ, P. A. 1988 The absolute and convective nature of instability in two-dimensional wakes at low Reynolds numbers. *Phys. Fluids* **31**, 999–1006.

PUJALS, G., COSSU, C. & DEPARDON, S. 2010*a* Forcing large-scale coherent streaks in a zero pressure gradient turbulent boundary layer. *J. Turbul.* **11** (25), 1–13.

PUJALS, G., DEPARDON, S. & COSSU, C. 2010*b* Drag reduction of a 3-D bluff body using coherent streamwise streaks. *Exp. Fluids* **49** (5), 1085–1094.

TANNER, M. 1972 A method of reducing the base drag of wings with blunt trailing edges. *Aeronaut. Q.* **23**, 15–23.

TOMBAZIS, N. & BEARMAN, P. W. 1997 A study of three-dimensional aspects of vortex shedding from a bluff body with a mild geometric disturbance. *J. Fluid Mech.* **330**, 85–112.